IEEE Access
Multidisciplinary | Rapid Review | Open Access Journal

Received February 1, 2022, accepted February 16, 2022, date of publication February 18, 2022, date of current version March 3, 2022.

Digital Object Identifier 10.1109/ACCESS.2022.3152785

A Selective Segmentation Model Using Dual-Level Set Functions and Local Spatial Distance

AFZAL RAHMAN[1], HAIDER ALI[1], NOOR BADSHAH[2], LAVDIE RADA[3], AYAZ ALI KHAN[4], HAMEED HUSSAIN[5], MUHAMMAD ZAKARYA[6], (Senior Member, IEEE), AFTAB AHMED[6], IZAZ UR RAHMAN[6], MUSHTAQ RAZA[6], AND MUHAMMAD HALEEM[7]

[1]Department of Mathematics, University of Peshawar, Peshawar 25120, Pakistan
[2]Department of Mathematics, University of Engineering and Technology Peshawar, Peshawar 25000, Pakistan
[3]Department of Mathematics, Bahcesehir University, 34349 Istanbul, Turkey
[4]Department of Computer Science, University of Lakki Marwat, Lakki Marwat 28420, Pakistan
[5]Department of Computer Science, University of Buner, Buner 19281, Pakistan
[6]Department of Computer Science, Abdul Wali Khan University Mardan, Mardan 23200, Pakistan
[7]Department of Computer Science, Kardan University, Kabul 1001, Afghanistan

Corresponding author: Muhammad Haleem (m.haleem@kardan.edu.af)

This work was supported in part by Kardan University, Kabul, Afghanistan; and in part by the University of Peshawar, Pakistan.

ABSTRACT Selective image segmentation is one of the most significant subjects in medical imaging and real-world applications. We present a robust selective segmentation model based on local spatial distance utilizing a dual-level set variational formulation in this study. Our concept tries to partition all objects using a global level set function and the selected item using a different level set function (local). Our model combines the marker distance function, edge detection, local spatial distance, and active contour without edges into one. The new model is robust to noise and gives better performance for images having intensity in-homogeneity (background and foreground). Moreover, we observed that the proposed model captures objects which do not have uniform features. The experimental results show that our model is robust to noise and works better than the other existing models.

INDEX TERMS Euler-Lagrange equation, selective segmentation, level set function, local spatial distance, local similarity factor.

I. INTRODUCTION

Image segmentation plays an important role in image processing and computer vision both. The aim of the image segmentation techniques is to differentiate various objects in the image foreground from the background; and consistently select special characteristics of an image that have enough features of interest. In addition, image segmentation has been widely used in a variety of applications, including medical imaging, object recognition, video analysis, traffic management systems, surveillance, and automated operations, to visualize relevant things in a given scene or picture.

For this purpose, different methods have been developed such as active contours and edge detection [1]–[3], region growing [4], [5], thresholding and histogram analysis [6]–[8]. In image segmentation, active contour models are widely studied and used due to their robustness and reliability. They are classified into two main categories that are region-based models [2], [9]–[11] and edge-based models [3], [12]–[14]. The region-based models use image intensities to guide the motion of active contours, while the edge-based models use edge information for guiding the active contours towards the object boundary. These models could segment all the features in a given image, which means that these are global segmentation models. However, they are not enough mature to overcome the problem of segmenting a particular object of interest in a given image.

In selective segmentation, the main problem is how to differentiate one feature from another if the objects have the similar/same intensity or the background and foreground are in-homogeneous with different intensities. For example, in Figure 18 the three objects have the same intensities, but in Figure 15 the intensities differences between the two objects are, extremely, small in a medical image. Moreover, as shown in Figure 13, three different images with multi objects, background, and foreground are in-homogeneous and have different intensities.

The associate editor coordinating the review of this manuscript and approving it for publication was Zhan-Li Sun.

In the literature, different techniques have been developed to overcome the selective segmentation problem such as graph-cut using graph cut theory [15], geodesics using edge-based function [16], and random walks using probability distributions [17]. Guyader *et al.* [18] proposed a model which is based on edge information of the object, while Badshah *et al.* [19] proposed a model which combines an edge-based model with region-based information. [18], [19] are useful and good work for a range of images. Badshah *et al.* [19] reproduced the same solution of the two piece-wise constants, however, if we solve in the time-marching framework, as in [2]; therefore, in this case, the capability of segmenting a particular object is lost, and we get a global segmentation. For successful segmentation and fast convergence, Nguyen *et al.* [20] combined the geometrical constraints and the Split Bregman method [21]. This model works properly if the object is smooth and well described by the weighted shortest boundary length. After all of this, Rada *et al.* [31] improved the models [18], [19], and competes the state-of-the-art model Nguyen *et al.* [20].

In this paper, we propose a variational model, which ensures better performance than the state-of-the-art models [31]–[33] for in-homogeneous, objects with the same/different intensities, in-homogeneous background, in-homogeneous foreground, and noisy images. At the same time, our model will handle two tasks, first global segmentation using region information, and second selective segmentation using both local region and local edge information. Dual-level set functions are employed because each task global function ψ_G and local function are characterized by level set function [22]–[26], [31]. The re-initialization may be required because the level set function is not unique. The local similarity factors (LSF) [34] depend on local spatial distance (to balance the intensity difference between the object and its neighbor) is incorporated in the proposed model to improve the segmentation results.

The rest of the paper is organized as follows. In Section II, we give a brief review of related models [31]–[33]. The proposed model and its Euler Lagrange equation are presented in Section III. For solving the PDE we describe an additive operator splitting method (AOS) in Section IV. In Section V, we presented some experimental results on different data set and compared with state-of-the-art models. Final remarks and conclusions are made in Section VI.

II. A REVIEW OF THE RELATED WORKS

As mentioned above, there are many variational (local and global) segmentation models. We will shortly summarize some of them related to this work. In the global segmentation, all objects in the image are segmented, while in selective segmentation one object of interest is segmented. For global segmentation, Mumford–Shah [9] is one of the most popular region-based model, for the best segmentation it aims to reconstruct a piece-wise smooth function to represent the given image. Using the piece-wise smooth function by Mumford–Shah [9] to find the edges of a given image, that varies over the image domain. But this model is computationally expensive and complex. A new variational global segmentation model is introduced by Chan-Vese [2], by replacing the piece-wise smooth function with a piece-wise constant function and the level set representation for intensities inside and outside the contour. It can detect contours without a gradient. This model may not efficiently segment images with intensity in-homogeneity or texture. To overcome such a problem, Ali *et al.* [27] introduced a global segmentation model based on generalized averages for segmentation of images having multiple objects and intensity in-homogeneity. But this model cannot segment a single object in the image having multi-objects. For this particular problem, there are many variational models [28]–[30] are introduced.

Mondal *et al.* [39] unveiled a new model that balances local and global data. For photos with in-homogeneous intensity, noise, and outliers, the model performs well. The model can handle intensity in-homogeneity pictures, hazy border or discontinuous edges, and the existence of moderated noise, according to the experimental findings demonstrated in various data sets. Chuang *et al.* [40] and Tripathy *et al.* [41] proposed models that are better for noisy MRI images but may not be as good for pictures with intensity in-homogeneity. Because this model is not convex, the initial guess must be adjusted multiple times until the desired results are obtained. Wu has suggested a convex variational segmentation model that ignores the factor and uses the idea of coefficient of variation (CoV). Wu *et al.* [42] has suggested a convex variational segmentation model based on the notion of coefficient of variation (CoV), which ignores the factor as well as the existence of noise and outliers in pictures. The fact that their CoV-based image data fitting term is sum of squares divided by sum of picture intensity supports this claim.

To introduce our new selective and global segmentation model, for segmenting the object of interest and all objects in a given image having intensity in-homogeneity, first we shortly summarize some selective segmentation models related to this work.

A. DUAL LEVEL-SET MODEL FOR SELECTIVE SEGMENTATION

Rada *et al.* [31], introduced a model for global and local selective segmentation, based on two level-sets, that is local and global level-sets. For local level sets, region-based terms are required for this model. Using $C_G = \partial\Omega_G$ in Ω for the global curve to locate the features of the image I, and $C_L = \partial\Omega_L$ in Ω for the desired selective curve, the Rada *et al.* [31] minimization equation is

$$
\begin{aligned}
&min_{\psi_L(x,y),\psi_G(x,y),e_1,e_2} F_\zeta(\psi_L(x,y),\psi_G(x,y),e_1,e_2)\\
&= \beta_1 \int_\Omega d(x,y)g(|\nabla I(x,y)|)\delta_\zeta(\psi_L(x,y))|\nabla\psi_L(x,y)|\\
&\quad \mathcal{H}_\zeta(\psi_G(x,y)+r)dxdy + \frac{\beta_L}{2}\int_\Omega (|\nabla\psi_L(x,y)|-1)^2 dxdy\\
&\quad +\beta_2 \int_\Omega g(|\nabla I(x,y)|)\delta_\zeta(\psi_G(x,y))|\nabla\psi_G(x,y)|dxdy + \frac{\beta_G}{2}
\end{aligned}
$$

$$\int_{\Omega}(|\nabla\psi_G(x,y)|-1)^2dxdy+\eta_{1G}\int_{\Omega}|I(x,y)-le_1|\mathcal{H}_\zeta(\psi_G(x,y))dxdy+\eta_{2G}\int_{\Omega}|I(x,y)-le_2|\times(1-\mathcal{H}_\zeta(\psi_G(x,y)))dxdy+\eta_1\int_{\Omega}|I(x,y)-le_1|\mathcal{H}_\zeta(\psi_L(x,y))dxdy+\eta_2\int_{\Omega}|I(x,y)-le_1|(1-\mathcal{H}_\zeta(\psi_L(x,y)))\mathcal{H}(\psi_G(x,y))dxdy+\eta_3\int_{\Omega}|I(x,y)-le_2|(1-\mathcal{H}_\zeta(\psi_L(x,y)))(1-\mathcal{H}_\zeta(\psi_G(x,y)))dxdy, \tag{1}$$

where β_1, β_2, β_L, β_G, η_{1G}, η_{2G}, η_1, η_2 and η_3 are all positive parameters, $d(x,y)$ is a distance function and g is the edge detector function defined in [19]. le_1, le_2 are the intensity means in the local interior and local exterior, respectively. Keeping ψ fixed and minimizing Eq. (1) with respect to le_1 and le_2, let $(1-\mathcal{H}_L(\psi_L))=Z_L$ we obtained the following equations:

$$le_1=\frac{\begin{bmatrix}\eta_{1G}\int_\Omega I\mathcal{H}_G(\psi_G)dxdy+\eta_1\int_\Omega I\mathcal{H}_L(\psi_L)dxdy\\+\eta_2\int_\Omega I(Z_L)\mathcal{H}_G(\psi_G)dxdy\end{bmatrix}}{\begin{bmatrix}\eta_{1G}\int_\Omega \mathcal{H}_G(\psi_G)dxdy+\eta_1\int_\Omega \mathcal{H}_L(\psi_L)dxdy\\+\eta_2\int_\Omega(Z_L)\mathcal{H}_G(\psi_G)dxdy\end{bmatrix}},$$

$$le_2=\frac{\begin{bmatrix}\eta_{2G}\int_\Omega I(1-\mathcal{H}_G(\psi_G))dxdy\\+\eta_3\int_\Omega I(1-\mathcal{H}_L(\psi_L))(1-\mathcal{H}_G(\psi_G))dxdy\end{bmatrix}}{\begin{bmatrix}\eta_{2G}\int_\Omega(1-\mathcal{H}_G(\psi_G))dxdy\\+\eta_3\int_\Omega(1-\mathcal{H}_L(\psi_L))(1-\mathcal{H}_G(\psi_G))dxdy\end{bmatrix}},$$

if the interior and exterior of $\psi_G(x,y)$ are non-empty. κ_σ is a Gaussian kernel function with the standard deviation σ. Keeping le_1, le_2 fixed, and minimizing Eq. (1) with respect to $\psi_L(x,y)$ and $\psi_G(x,y)$.

$$\begin{cases}\beta_1\delta_\zeta(\psi_L)\nabla\left(\mathcal{W}\mathcal{H}_\zeta(\psi_G+r)\dfrac{\nabla\psi_L}{|\nabla\psi_L|}\right)\\+\beta_L\nabla\left(\left(1-\dfrac{1}{|\nabla\psi_L|}\right)\nabla\psi_L\right)\\+\delta_\zeta(\psi_L)(-\eta_1(I(x,y)-le_1)^2+\eta_2(I(x,y)-le_1)^2\\\mathcal{H}_\zeta\psi_G+\eta_3(I(x,y)-le_2)^2(1-\mathcal{H}_\zeta(\psi_G)))=0,\ \text{in }\Omega,\\\dfrac{\partial\psi_L}{\partial\vec{m}}=0,\ \text{on }\Omega,\end{cases} \tag{2}$$

$$\begin{cases}\beta_2\delta_\zeta(\psi_G)\nabla\left(g(x,y)\dfrac{\nabla\psi_G}{|\nabla\psi_G|}\right)\\+\beta_G\nabla\left(\left(1-\dfrac{1}{|\nabla\psi_G|}\right)\nabla\psi_G\right)\\+\delta_\zeta(\psi_G+r)(-\eta_1\mathcal{W}(x,y)|\nabla\mathcal{H}_\zeta(\psi_L)|)\\+\delta_\zeta(\psi_G)(-\eta_{1G}(I(x,y)-le_1)^2\\+\eta_{2G}(I(x,y)-le_2)^2-\eta_2(I(x,y)-le_2)^2(1-\mathcal{H}\psi_G))\\+\eta_3(I(x,y)-le_2)^2(1-\mathcal{H}(\psi_L))=0,\ \text{in }\Omega,\\\dfrac{\partial\psi_G}{\partial\vec{m}}=0,\ \text{on }\Omega,\end{cases} \tag{3}$$

where $\mathcal{W}=dg(\nabla I)$.

This model may not work well for images with intensity in-homogeneity and noise, for examples Figs. 11 and 12.

B. TEXTURAL AND IN-HOMOGENEOUS OBJECT EXTRACTION MODEL

For the segmentation of multiple objects with intensity difference and in-homogeneity, Mabood *et al.* [32] introduced a selective segmentation model. This model is based on the average image of channels (AIC), and segment images having texture and noise. For texture image segmentation, the authors utilize the extended structure tensor (EST) in order to obtain the AIC.

The classical structure tensor (CST) J_σ is given by Gaussian smoothing of tensor product of the image gradient,

$$J_\sigma=\kappa_\sigma\star(\nabla z\nabla z^\tau)=\begin{pmatrix}\kappa_\sigma\star I_x^2 & \kappa_\sigma\star I_xI_y\\ \kappa_\sigma\star I_xI_y & \kappa_\sigma\star I_y^2\end{pmatrix} \tag{4}$$

κ_σ is a Gaussian kernel function with standard deviation σ, x, y in the subscript denote the partial derivatives.

The EST J_σ^E for a gray-scale image I defined by

$$J_\sigma^E=\kappa_\sigma\star(uu^\tau)=\begin{pmatrix}\kappa_\sigma\star I_x^2 & \kappa_\sigma\star I_xI_y & \kappa_\sigma\star I_xI\\ \kappa_\sigma\star I_xI_y & \kappa_\sigma\star I_y^2 & \kappa_\sigma\star I_yI\\ \kappa_\sigma\star I_xI & \kappa_\sigma\star I_yI & \kappa_\sigma\star I^2\end{pmatrix} \tag{5}$$

where $u=[z_x\quad z_y\quad z]^\tau$. By Computing the EST one can obtain the AIC of all the channels $J_{\sigma,i}^E\in J_\sigma^E$ for $i=1,2,\ldots,9$. The AIC is given by:

$$\zeta^*=\frac{1}{9}\sum_{i=1}^{9}J_{\sigma,i}^E. \tag{6}$$

Mabood *et al.* [32] minimization functional as follows:

$$F^{2D}=\mu\int_\Omega d(x,y)g(|\nabla z|)\delta\psi|\nabla(\psi)|dxdy+\lambda D(\zeta^*(x,y)), \tag{7}$$

where the first term is the edge detector function and blends of metric, while the second term is the data term which uses the information from the AIC to tackle textural and noisy objects of interest. The data term D performs better for detecting homogeneous intensity objects and is robust against noise [19], but for the images with intensity in-homogeneity, the performance is poor.

C. WEIGHTED VARIATIONAL MODEL FOR SELECTIVE IMAGE SEGMENTATION (Liu)

Liu *et al.* [33] proposed a model, which applies the weighting ω to the data fitting terms for adjusting the fidelity and smoothing terms, and the minimization problem is given by

$$F(u)=\mu\int_\Omega|\nabla u|d\Omega+\mu_2\int_\Omega|\nabla u|^2d\Omega+\lambda\int_\Omega\omega^2(x,y)|z-u|^2d\Omega, \tag{8}$$

where the parameters $\mu,\mu_2,\lambda\geq 0$, $\omega(x,y)=1-D(x,y)g(|\nabla z|)$, D is a distance function from marker set M (see [33]).

D. SELECTIVE SEGMENTATION MODEL FOR MULTI-REGIONS WITHIN THE OBJECT OF INTEREST

Ali *et al.* [38] proposed a selective segmentation model based on generalized averages, the minimization functional is given by:

$$\begin{aligned} F(e_2,\psi) = \mu\int_\Omega d(x,y)g(|\nabla I(x,y)|)\delta_\zeta(\psi)|\nabla\psi|dxdy \\ +\eta_1\int_\Omega |I(x,y)-le_1|^2\mathcal{H}_\zeta(\psi)dxdy \\ +\eta_2\int_\Omega |I(x,y)-le_1|^2(1-\mathcal{H}_\zeta(\psi))dxdy \\ +\nu\left(\int_\Omega \mathcal{H}_\zeta(\psi(x,y))dxdy - A_1\right)^2 \\ +\nu\left(\int_\Omega (1-\mathcal{H}_\zeta(\psi(x,y)))dxdy - A_2\right), \quad (9) \end{aligned}$$

where the parameters μ, η_1, η_2 and ν are non-negative, g is the edge detector function, d is a distance function, A_1, A_2 are the areas inside and outside the initial polygon respectively, le_1 is the generalized mean of the polygon constructed with the help of markers, le_2 is the generalized mean intensity outside the desired object, ψ is a level set function and $\mathcal{H}_\zeta$ is the regularized Heaviside function.

They aims that the method is working good for detecting single-region and an outperforming for multi-region selective segmentation.

III. PROPOSED MODEL

Motivated by the local and global region-based active contour models [15], [18], they may fail to segment images with the in-homogeneous intensities, or if the intensity difference between two objects is very small. We proposed a new efficient and robust region-based model for noisy images having intensities homogeneous and in-homogeneous.

Let us denote the given image by I, the global evolving curve by $C_G = \partial\Omega_G$ in Ω, and the desired selective curve by $C_L = \partial\Omega_L$ in Ω. Assume that $\Omega_L \subset \Omega_G$, this implies that $in(C_L) = \Omega_L$, $out(C_L) = \Omega\backslash\bar{\Omega}_L$, $in(C_G) = \Omega_G$, $out(C_G) = \Omega\backslash\bar{\Omega}_G$. Defining the two zero level set functions $\psi_L(x,y)$ and $\psi_G(x,y)$ by:

$$\begin{cases} C_L = \partial\Omega_L = \{(x,y)\in\Omega : \psi_L(x,y) = 0\}, \\ in(C_L) = \Omega_L = \{(x,y)\in\Omega : \psi_L(x,y) > 0\}, \\ out(C_L) = \Omega\backslash\bar{\Omega}_L = \{(x,y)\in\Omega : \psi_L(x,y) < 0\}. \end{cases}$$

$$\begin{cases} C_G = \partial\Omega_G = \{(x,y)\in\Omega : \psi_G(x,y) = 0\}, \\ in(C_G) = \Omega_G = \{(x,y)\in\Omega : \psi_G(x,y) > 0\}, \\ out(C_G) = \Omega\backslash\bar{\Omega}_G = \{(x,y)\in\Omega : \psi_G(x,y) < 0\}. \end{cases}$$

In such a way, the unknown quantities C_L, C_G are replaced respectively by ψ_L, ψ_G. To seek the possible advantages of having expanded domain of Ω_G within a distance r, define

$$\Omega_{G,r} = \{(x,y)\in\Omega : \psi_G(x,y) > -r\},$$

where the parameter $r = 0$ or $r = 3$, and $\Omega_L \subset \Omega_G \subseteq \Omega_{G,r} \subset \Omega$.

By keeping in mind the idea of searching selective features Ω_L in the local domain Ω_G, and all features Ω_G in the whole image domain Ω, we consider a new variational model:

$$\begin{aligned} &min_{C_L,C_G,e_1,e_2}F(C_L,C_G,e_1,e_2) \\ &= \beta_1\int_{C_L} d(x,y)g(|\nabla I(x,y)|)ds + \beta_2\int_{C_G} g(|\nabla I(x,y)|)ds \\ &\quad +\eta_{1G}\int_{inside(C_G)} |I(x,y)-e_1|^2dxdy + \eta_{2G}\int_{outside(C_G)} \\ &\quad |I(x,y)-e_2|^2dxdy + \eta_1\int_{inside(C_L)} |I(x,y)-e_1|^2dxdy \\ &\quad +\eta_2\int_{outside(C_L)\cap inside(C_G)} |I(x,y)-e_1|^2dxdy \\ &\quad +\eta_3\int_{outside(C_L)\cap outside(C_G)} |I(x,y)-e_2|^2dxdy, \quad (10) \end{aligned}$$

where

$$g(|\nabla I(x,y)|) = \frac{1}{1+|\nabla G_\sigma(x,y)*I(x,y)|^2}, \quad (11)$$

β_1, β_2, η_{1G}, η_{2G}, η_1, η_2 and η_3 are all positive parameters, $d(x,y)$ is distance function defined in [19]. $G_\sigma(x,y)*I(x,y)$ is a smooth version of $I(x,y)$ with the Gaussian kernel $G_\sigma(x,y) = \sigma^{\frac{-1}{2}}exp^{\frac{-|x^2+y^2|}{4\sigma}}$ to control the possible noise. To derive the level set formulation for the Eq. (10), first $\psi_L(x,y)$ and $\psi_G(x,y)$ will be scaled automatically with new term as in [14]. For computing the weight length of C_L to $\Omega_{G,r}$ in place of Ω we compel the search domain,

$$\begin{aligned} &\int_{C_L} d(x,y)g(|\nabla I(x,y)|)ds \\ &= \int_\Omega d(x,y)g(|\nabla I(x,y)|)|\nabla\mathcal{H}(\psi_L(x,y))|dxdy \\ &\quad +\int_{\Omega_{G,r}} d(x,y)g(|\nabla I(x,y)|)|\nabla\mathcal{H}(\psi_L(x,y))|dxdy \\ &\quad +\int_\Omega d(x,y)g(|\nabla I(x,y)|)|\nabla\mathcal{H}(\psi_L(x,y))|\mathcal{H}(\psi_G(x,y)+r) \\ &\quad dxdy. \quad (12) \end{aligned}$$

Replacing the non-differentiable function $\mathcal{H}$ by regularized Heaviside function $\mathcal{H}_\zeta$ as in [1], [2]. We will use the following Heaviside functions

$$\mathcal{H}_{1\zeta} = \begin{cases} 0, & z < -\zeta \\ \frac{1}{2}\left[1+\frac{z}{\zeta}+\frac{1}{\pi}cos\frac{\pi z}{\zeta}\right], & |z|\le\zeta \\ 1, & z > \zeta \end{cases}$$

$$\mathcal{H}_{2\zeta} = \frac{1}{2}\left(1+erf\left(\frac{\zeta}{z}\right)\right),$$

$$\mathcal{H}_{3\zeta} = \frac{1}{2}\left(1+\frac{2}{\pi}arctan\left(\frac{z}{\zeta}\right)\right)$$

where the gauss error function ($erf(y)$) is double of the integral of Gaussian distribution $\mathcal{N}(0,\frac{1}{2})$ having the form:

$$erf(y) = \frac{2}{\sqrt{\pi}}\int_0^y e^{-t^2}dt.$$

The function $\mathcal{H}_{1\zeta}$, $\mathcal{H}_{2\zeta}$ and its corresponding delta functions $\delta_{1\zeta}$, $\delta_{2\zeta}$ have small support in the interval $[-\zeta, \zeta]$, but $\mathcal{H}_{3\zeta}$ and $\delta_{3\zeta}$ are non-zero all over. We suggest to use $\mathcal{H}_{1\zeta}$ or $\mathcal{H}_{2\zeta}$ because $\delta_{3\zeta}$ may not be good for the case where the features of interest is lower than two pixels aside from other features, the problem will be resolved if we adjust ζ while we lose the automatic efficiency.

The Eq. (10) with the regularized Heaviside function and local similarity factor in [34], can be written as:

$$
\begin{aligned}
&min_{\psi_L(x,y),\psi_G(x,y),e_1,e_2} F_\zeta(\psi_L(x,y),\psi_G(x,y),e_1,e_2)\\
&= \beta_1 \int_\Omega d(x,y) g(|\nabla I(x,y)|)\delta_\zeta(\psi_L(x,y))|\nabla\psi_L(x,y)|\\
&\quad \mathcal{H}_\zeta(\psi_G(x,y)+r)dxdy + \frac{\beta_L}{2}\int_\Omega (|\nabla\psi_L(x,y)|-1)^2 dxdy\\
&\quad +\beta_2 \int_\Omega g(|\nabla I(x,y)|)\delta_\zeta(\psi_G(x,y))|\nabla\psi_G(x,y)|dxdy\\
&\quad +\frac{\beta_G}{2}\int_\Omega (|\nabla\psi_G(x,y)|-1)^2 dxdy + \eta_{1G}\int_{(y\in N_x)\neq x}\\
&\quad \frac{|I(x,y)-le_1|^2}{d(x,y)}\mathcal{H}_\zeta(\psi_G(x,y))dxdy + \eta_{2G}\int_{(y\in N_x)\neq x}\\
&\quad \frac{|I(x,y)-le_2|^2}{d(x,y)}(1-\mathcal{H}_\zeta(\psi_G(x,y)))dxdy + \eta_1\int_{(y\in N_x)\neq x}\\
&\quad \frac{|I(x,y)-le_1|^2}{d(x,y)}\mathcal{H}_\zeta(\psi_L(x,y))dxdy + \eta_2\int_{(y\in N_x)\neq x}\\
&\quad \frac{|I(x,y)-le_1|^2}{d(x,y)}(1-\mathcal{H}_\zeta(\psi_L(x,y)))\mathcal{H}(\psi_G(x,y))dxdy\\
&\quad +\eta_3\int_{(y\in N_x)\neq x}\frac{|I(x,y)-le_2|^2}{d(x,y)}(1-\mathcal{H}_\zeta(\psi_L(x,y)))\\
&\quad (1-\mathcal{H}_\zeta(\psi_G(x,y)))dxdy,
\end{aligned}
\tag{13}
$$

where $\beta_L > 0$, $\beta_G > 0$ and le_1, le_2 are the intensity means in the local interior and local exterior respectively. N_x is a neighborhood of x. Simply we will write d, I, ψ_L and ψ_G for $d(x,y)$, $I(x,y)$, $\psi_L(x,y)$ and $\psi_G(x,y)$ respectively. Assume that $\psi_G(x,y)$ has neither empty interior nor empty exterior, then keeping ψ fixed and minimizing Eq. (13) with respect to le_1 and le_2, we obtained the following equations:

$$
le_1 = \frac{\kappa_\sigma * \begin{bmatrix}\eta_{1G}(I\mathcal{H}_G(\psi_G)) + \eta_1(I\mathcal{H}_L(\psi_L))\\ +\eta_2(I(1-\mathcal{H}_L(\psi_L)))\mathcal{H}_G(\psi_G)\end{bmatrix}}{\kappa_\sigma * \begin{bmatrix}\eta_{1G}(1\mathcal{H}_G(\psi_G)) + \eta_1(1\mathcal{H}_L(\psi_L))\\ +\eta_2(1-\mathcal{H}_L(\psi_L))\mathcal{H}_G(\psi_G)\end{bmatrix}}, \tag{14}
$$

$$
le_2 = \frac{\kappa_\sigma * \begin{bmatrix}\eta_{2G}(I(1-\mathcal{H}_G(\psi_G)))\\ +\eta_3(I(1-\mathcal{H}_L(\psi_L)))(1-\mathcal{H}_G(\psi_G))\end{bmatrix}}{\kappa_\sigma * \begin{bmatrix}\eta_{2G}(1-\mathcal{H}_G(\psi_G))\\ +\eta_3(1-\mathcal{H}_L(\psi_L))(1-\mathcal{H}_G(\psi_G))\end{bmatrix}}, \tag{15}
$$

κ_σ is a Gaussian kernel function with the standard deviation σ.

Keeping le_1, le_2 fixed, and minimizing Eq. (13) with respect to $\psi_L(x,y)$ and $\psi_G(x,y)$. To find the first variation of F_ζ with respect to ψ_L, we minimize F_ζ with respect to ψ_L by using the Gâteaux derivative

$$
\lim_{h\to 0}\frac{d}{dh}(F_\zeta(\psi_L + h\phi, le_1, le_2)) = 0.
$$

Following the same procedure as in [19], we get the Euler-Lagrange equation for ψ_L:

$$
\begin{cases}
\beta_1\delta_\zeta(\psi_L)\nabla\left(\mathcal{W}\mathcal{H}_\zeta(\psi_G+r)\dfrac{\nabla\psi_L}{|\nabla\psi_L|}\right)\\
+\beta_L\nabla\left(\left(1-\dfrac{1}{|\nabla\psi_L|}\right)\nabla\psi_L\right)\\
+\delta_\zeta(\psi_L)(-\eta_1(I(x,y)-le_1)^2\\
+\eta_2(I(x,y)-le_1)^2\mathcal{H}_\zeta\psi_G\\
+\eta_3(I(x,y)-le_2)^2(1-\mathcal{H}_\zeta(\psi_G))) = 0, \text{ in } \Omega,\\
\dfrac{\partial\psi_L}{\partial\vec{m}} = 0, \text{ on } \Omega,
\end{cases}
\tag{16}
$$

where $\mathcal{W} = d(x,y)g(\nabla I(x,y))$ and the boundary conditions reduce to Neumann boundary conditions:

$$
\beta_1\mathcal{W}\mathcal{H}_\zeta(\psi_G+r)\frac{\delta_\zeta(\psi_L)}{|\nabla\psi_L|}\frac{\partial\psi_L}{\partial\vec{m}} = 0
$$

and

$$
\beta_L(|\psi_L|-1)\frac{1}{|\nabla\psi_L|}\frac{\partial\psi_L}{\partial\vec{m}} = 0.
$$

By the same procedure, we can get the Euler-Lagrange equation for ψ_G.

To speedify the convergence, we add the ballon terms $\alpha\mathcal{W}|\nabla\psi_L|, \alpha g(x,y)|\nabla\psi_G|$ in equation for ψ_L and ψ_G respectively. So the equation for ψ_L and ψ_G are:

$$
\begin{cases}
\beta_1\delta_\zeta(\psi_L)\nabla\left(\mathcal{W}\mathcal{H}_\zeta(\psi_G+r)\frac{\nabla\psi_L}{|\nabla\psi_L|}\right)\\
+\beta_L\nabla\left(\left(1-\frac{1}{|\nabla\psi_L|}\right)\nabla\psi_L\right)\\
+\delta_\zeta(\psi_L)(-\eta_1(I(x,y)-le_1)^2\\
+\eta_2(I(x,y)-le_1)^2\mathcal{H}_\zeta\psi_G + \eta_3(I(x,y)-le_2)^2\\
(1-\mathcal{H}_\zeta(\psi_G))) + \alpha\mathcal{W}(x,y)|\nabla\psi_L| = 0, \text{ in } \Omega,\\
\frac{\partial\psi_L}{\partial\vec{m}} = 0, \text{ on } \Omega,
\end{cases}
\tag{17}
$$

$$
\begin{cases}
\beta_2\delta_\zeta(\psi_G)\nabla\left(g(x,y)\frac{\nabla\psi_G}{|\nabla\psi_G|}\right)\\
+\beta_G\nabla\left(\left(1-\frac{1}{|\nabla\psi_G|}\right)\nabla\psi_G\right)\\
+\delta_\zeta(\psi_G+r)(-\eta_1\mathcal{W}(x,y)|\nabla\mathcal{H}_\zeta(\psi_L)|)\\
+\delta_\zeta(\psi_G)(-\eta_{1G}(I(x,y)-le_1)^2 + \eta_{2G}(I(x,y)-le_2)^2\\
-\eta_2(I(x,y)-le_2)^2(1-\mathcal{H}\psi_G)) + \eta_3(I(x,y)-le_2)^2\\
(1-\mathcal{H}(\psi_L)) + \alpha g(x,y)|\nabla\psi_G| = 0, \text{ in } \Omega,\\
\frac{\partial\psi_G}{\partial\vec{m}} = 0, \text{ on } \Omega.
\end{cases}
\tag{18}
$$

To get the linear system of equations, we freeze the non-linear coefficients in Eqs. (17) and (18), then it can be solved by the fixed point method. The deficiency of the fixed point method is the computational cost of the related linear system for large images. We develop a fast technique analogously to [2], [19], [36].

IV. SOLUTION OF THE PROPOSED METHOD

For solving Eqs. (17) and (18), we choose an efficient additive operator splitting technique (AOS) [35], [36] which is low computationally cost and fast convergent. Consider the parabolic equations related to Eqs. (17) and (18) respectively.

$$\begin{cases} \psi_L(x,y,0) = \psi_L^0(x,y) \\ \dfrac{\partial \psi_L}{\partial \tau} = \beta_1 \delta_\zeta(\psi_L)\nabla\left(\mathcal{W}\mathcal{H}_\zeta(\psi_G + r)\dfrac{\nabla\psi_L}{|\nabla\psi_L|}\right) \\ +\beta_L\nabla\left(\left(1 - \dfrac{1}{|\nabla\psi_L|}\right)\nabla\psi_L\right) + \delta_\zeta(\psi_L) \\ \times(-\eta_1(I(x,y) - le_1)^2 + \eta_2(I(x,y) - le_1)^2 \\ \times\mathcal{H}_\zeta(\psi_G) + \eta_3(I(x,y) - le_2)^2 \\ \times(1 - \mathcal{H}_\zeta(\psi_G))) + \alpha\mathcal{W}(x,y)|\nabla\psi_L|, \\ \dfrac{\partial \psi_L}{\partial \vec{m}}|_{\partial\Omega} = 0, \end{cases} \tag{19}$$

$$\begin{cases} \psi_G(x,y,0) = \psi_G^0(x,y) \\ \dfrac{\partial \psi_G}{\partial \tau} = \beta_2 \delta_\zeta(\psi_G)\nabla\left(g(x,y)\dfrac{\nabla\psi_G}{|\nabla\psi_G|}\right) + \beta_G\nabla \\ \times\left(\left(1 - \dfrac{1}{|\nabla\psi_G|}\right)\nabla\psi_G\right) + \delta_\zeta(\psi_G + r) \\ \times(-\eta_1\mathcal{W}(x,y)|\nabla\mathcal{H}_\zeta(\psi_L)|) + \alpha g(x,y) \\ \times|\nabla\psi_G| + \delta_\zeta(\psi_G)(-\eta_{1G}(I(x,y) - le_1)^2 \\ +\eta_{2G}(I(x,y) - le_2)^2 - \eta_2(I(x,y) - le_2)^2 \\ \times(1 - \mathcal{H}\psi_L)) + \eta_3(I(x,y) - le_2)^2 \\ \times(1 - \mathcal{H}(\psi_L)), \\ \dfrac{\partial \psi_G}{\partial \vec{m}}|_{\partial\Omega} = 0. \end{cases} \tag{20}$$

Let's denote this by:

$$\begin{aligned} h_L &= \delta_\zeta(\psi_L)(-\eta_1(I(x,y) - le_1)^2 + \eta_2(I(x,y) - le_1)^2 \\ &\quad \times\mathcal{H}_\zeta(\psi_G) + \eta_3(I(x,y) - le_2)^2(1 - \mathcal{H}_\zeta(\psi_G))) \\ &\quad +\alpha\mathcal{W}(x,y)|\nabla\psi_L|, \\ h_G &= \delta_\zeta(\psi_G + r)(-\eta_1\mathcal{W}(x,y)\mathcal{H}_\zeta(\psi_L)) + \delta_\zeta(\psi_G)(-\eta_{1G} \\ &\quad \times(I(x,y) - le_1)^2 + \eta_{2G}(I(x,y) - le_2)^2 - \eta_2 \\ &\quad \times(I(x,y) - le_1)^2(1 - \mathcal{H}\psi_L)) + \eta_3(I(x,y) - le_2)^2 \\ &\quad \times(1 - \mathcal{H}(\psi_L)) + \alpha g(x,y)|\nabla\psi_G|, \\ \mathcal{F}_L &= \frac{\mathcal{W}\mathcal{H}_\zeta(\psi_G + r)}{|\nabla\psi_L|}, \quad \mathcal{F}_G = \frac{g}{|\nabla\psi_G|}, \\ \mathcal{H}_L &= 1 - \frac{1}{|\nabla\psi_L|} \\ \mathcal{H}_G &= 1 - \frac{1}{|\nabla\psi_G|}. \end{aligned}$$

So the compact form of Eqs. (19) and (20) can be written as:

$$\begin{cases} \frac{\partial \psi_L}{\partial \tau} = \beta_1\delta_\zeta(\psi_L)\nabla(\mathcal{F}_L\nabla\psi_L) + \beta_L\nabla(\mathcal{H}_L\nabla\psi_L) + h_L \\ = \beta_1\delta_\zeta(\psi_L)(\partial_x(\mathcal{F}_L\partial_x\psi_L) + \partial_y(\mathcal{F}_L\partial_y\psi_L)) \\ +\beta_L(\partial_x(\mathcal{H}_L\partial_x\psi_L) + \partial_y(\mathcal{H}_L\partial_y\psi_L)) + h_L, \\ \frac{\partial \psi_G}{\partial \tau} = \beta_2\delta_\zeta(\psi_G)\nabla(\mathcal{F}_G\nabla\psi_G) + \beta_G\nabla(\mathcal{H}_G\nabla\psi_G) + h_G \\ = \beta_2\delta_\zeta(\psi_G)(\partial_x(\mathcal{F}_G\partial_x\psi_G) + \partial_y(\mathcal{F}_G\partial_y\psi_G)) \\ +\beta_G(\partial_x(\mathcal{H}_G\partial_x\psi_G) + \partial_y(\mathcal{H}_G\partial_y\psi_G)) + h_G. \end{cases} \tag{21}$$

We have to iterate Eq. (21) because it has nonlinear coefficients and ψ_L, ψ_G are dependent on each other. Both the equations in Eq. (21) are of the same disjoint form. It will be enough to solve the second equation:

$$\begin{aligned} \frac{\partial \psi_G}{\partial \tau} &= \beta_2\delta_\zeta(\psi_G)(\partial_x(\mathcal{F}_G\partial_x\psi_G) + \partial_y(\mathcal{F}_G\partial_y\psi_G)) \\ &\quad +\beta_G(\partial_x(\mathcal{H}_G\partial_x\psi_G) + \partial_y(\mathcal{H}_G\partial_y\psi_G)) + h_G \end{aligned} \tag{22}$$

In x coordinate direction,the semi implicit form of Eq. (22) for a step size $s_1 = s_2 = s = 1$,

$$\begin{aligned} &\frac{\psi_{i,j}^{k+1} - \psi_{i,j}^k}{2\nabla\tau} \\ &= \beta_2\delta_\zeta(\psi_{i,j})\left(\left(\frac{\mathcal{F}_{i,j}^k + \mathcal{F}_{i+1,j}^k}{2s^2}\right)(\psi_{i+1,j}^{k+1} - \psi_{i,j}^{k+1})\right) \\ &\quad -\beta_2\delta_\zeta(\psi_{i,j})\left(\left(\frac{\mathcal{F}_{i,j}^k + \mathcal{F}_{i-1,j}^k}{2s^2}\right)(\psi_{i,j}^{k+1} - \psi_{i-1,j}^{k+1})\right) \\ &\quad +\beta_G\left(\left(\frac{\mathcal{H}_{i,j}^k + \mathcal{H}_{i+1,j}^k}{2s^2}\right)(\psi_{i+1,j}^{k+1} - \psi_{i,j}^{k+1})\right) \\ &\quad -\beta_G\left(\left(\frac{\mathcal{H}_{i,j}^k + \mathcal{H}_{i-1,j}^k}{2s^2}\right)(\psi_{i,j}^{k+1} - \psi_{i-1,j}^{k+1})\right) \\ &\quad +\frac{1}{2}h_{i,j}, \end{aligned} \tag{23}$$

$$\begin{aligned} &\Longrightarrow \psi_{i,j}^{k+1} \\ &= \psi_{i,j}^k + 2\nabla\tau(v_1\psi_{i+1,j}^{k+1} - v_2\psi_{i,j}^{k+1} + v_3\psi_{i-1,j}^{k+1}) \\ &\quad +\nabla\tau h_{i,j}, \end{aligned} \tag{24}$$

where

$$v_1 = \beta_2\delta_\zeta(\psi_{i,j})\frac{\mathcal{F}_{i,j}^k + \mathcal{F}_{i+1,j}^k}{2s^2} + \beta_G\frac{\mathcal{H}_{i,j}^k + \mathcal{H}_{i+1,j}^k}{2s^2}, \tag{25}$$

$$\begin{aligned} v_2 &= \beta_2\delta_\zeta(\psi_{i,j})\frac{\mathcal{F}_{i-1,j}^k + 2\mathcal{F}_{i,j}^k + \mathcal{F}_{i+1,j}^k}{2s^2} \\ &\quad +\beta_G\frac{\mathcal{H}_{i-1,j}^k + 2\mathcal{H}_{i,j}^k + \mathcal{H}_{i+,j}^k}{2s^2}, \end{aligned} \tag{26}$$

$$v_3 = \beta_2\delta_\zeta(\psi_{i,j})\frac{\mathcal{F}_{i,j}^k + \mathcal{F}_{i-1,j}^k}{2s^2} + \beta_G\frac{\mathcal{H}_{i,j}^k + \mathcal{H}_{i-1,j}^k}{2s^2}. \tag{27}$$

In the same way, in y coordinate direction:

$$\begin{aligned} \Longrightarrow \psi_{i,j}^{k+1} &= \psi_{i,j}^k + 2\nabla\tau(\bar{v}_1\psi_{i,j+1}^{k+1} - \bar{v}_2\psi_{i,j}^{k+1} \\ &\quad +\bar{v}_3\psi_{i,j-1}^{k+1}) + \nabla\tau h_{i,j}. \end{aligned} \tag{28}$$

Solving the uncoupled system of Eqs. (24) and (28) in the equality of AOS, with the time step $2\nabla\tau$ in the directions of x, y respectively, and then take the mean of the two solutions with the result equivalent to a coupled semi-implicit system and time step $\nabla\tau$. The matrix form of Eqs.(24) and (28) is:

$$(I - 2\nabla\tau B_{\mathcal{I}}(\psi^k))\psi_{\mathcal{I}}^{k+1} = \hat{h}^k, \quad \text{for } \mathcal{I} = 1, 2.$$

$$\psi^{k+1} = \frac{1}{2}\sum_{i=1}^{2}\psi_{\mathcal{I}}^{k+1}, \quad k = 1, 2, \ldots,$$

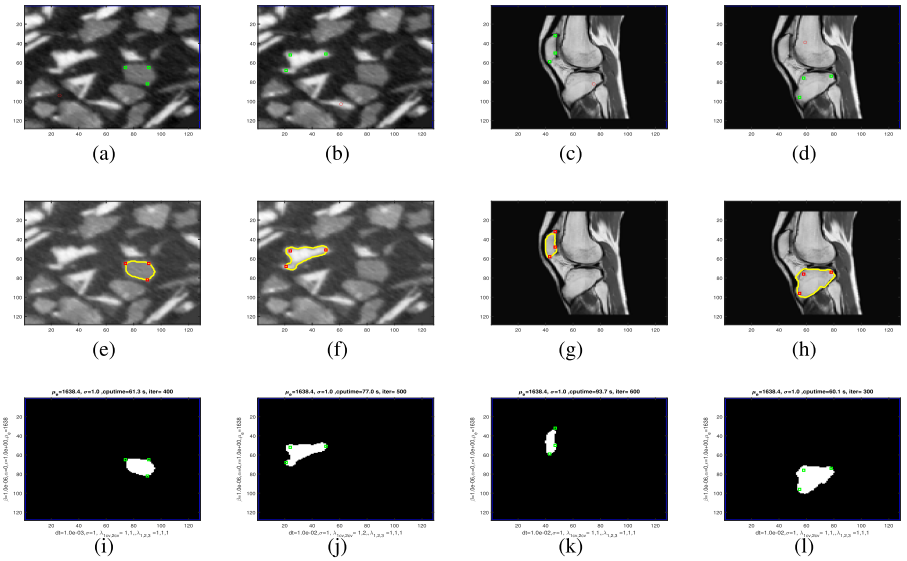

FIGURE 1. (a-d) Tomographic and medical images with markers, (e-h) successful Local segmentation and (i-l) segmented features with $dt = 0.01$.

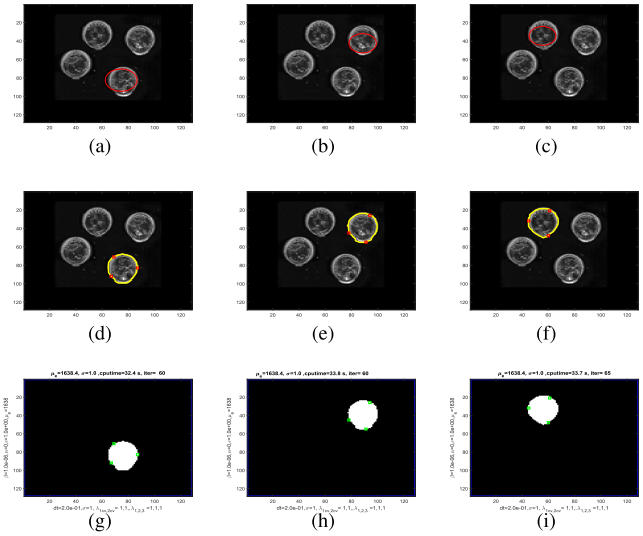

FIGURE 2. Performance of the proposed method for Image with a noise (salt and pepper noise) density of 0.02. (a-c) Noisy images with initial contour, (d-f) successful Local segmentation results and (g-i) segmented features with $dt = 0.2$.

where $\mathcal{I}$ is the identity matrix, $\hat{h}^k = \psi^k + \nabla\tau h^k$, $B_{\mathcal{I}}$ is a tri-diagonal matrix containing $(v_1, -v_2, v_3)$ and $\bar{v_1}, -\bar{v_2}, \bar{v_3}$ respectively for $\mathcal{I} = 1, 2$.

V. EXPERIMENTAL RESULTS

This section includes experimental results to clarify the performance, robustness, and accuracy of the proposed model, also some comparison with the exiting models [31]–[33] on homogeneous, in-homogeneous, and noisy images. We executed the experiment on medical, synthetic, artificial, and real images with different shapes and contours. The test images are taken from the datasets available online at kaggle.[1]

[1]https://www.kaggle.com/

TABLE 1. Efficiency comparison of the proposed model with Rada *et al.* [31] on 10 different images.

Figure	proposed model		Rada et al.	
	Iter.	CPU (sec)	Iter.	CPU (sec)
3	600	144.5	650	157.4
4	221	67.8	500	145.2
5	200	67.0	200	72.1
6	500	70.0	500	80.8
7	100	41.6	200	67.9
8	300	94.8	350	110.3
9	350	99.1	350	120.4
10	500	126.9	600	136.7
11	500	138.1	600	140.2
12	300	88.6	300	96.3

The better performance of our proposed model in terms of efficiency, quality, robustness, and speed will be observed. All the experiments were carried out using Matlab 9.10.0 on a core $i7$ computer with $8GB$ RAM, $2.70GHz$ processor, window 10 operating system. The image size choose 128 or 256 and the parameters are $\eta_1 = \eta_2 = \eta_3 = 1$, $\eta_{1G} = \eta_{1G} = 1$, $\tau = 4$, step space $h = 1$, time step $\nabla t = 0.1$ or 0.01 or 0.001 or 0.2, $\alpha = 0.001$, $\eta_L = \eta_G = 0.4$, $\beta_1 = \beta_2 = \frac{m^2}{10}$. The initial global and local level sets have the form:

$$\psi_G^0 = \sqrt{(x - x_G^0)^2(y - y_G^0)^2} - r_G^0$$
$$\psi_L^0 = \sqrt{(x - x_L^0)^2(y - y_L^0)^2} - r_L^0,$$

where (x_G^0, y_G^0), (x_L^0, y_L^0) are the center of the circle and center of the markers in a set D, respectively. Moreover, $r_G^0 = \frac{m}{5}$ is radius, $r_L^0 = min_{a \neq b}||p_a - p_b||$ is the minimum distance of the markers, $a, b \in D$, where

$$x_L^0 = \frac{\sum x}{n(markers)} \quad y_L^0 = \frac{\sum y}{n(markers)}.$$

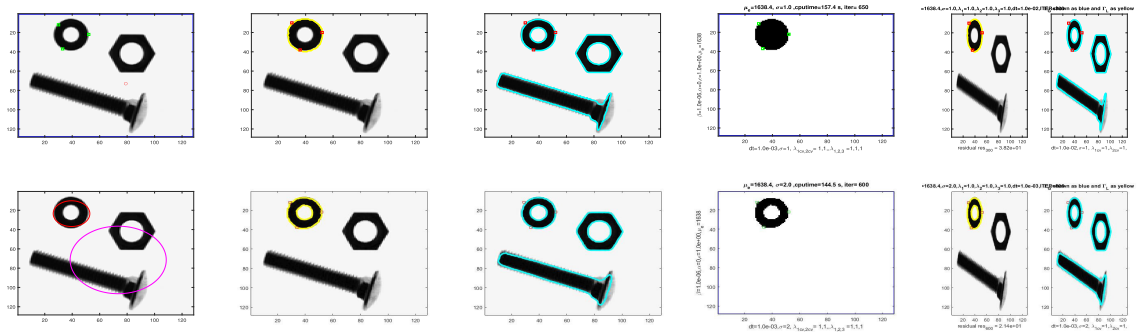

FIGURE 3. For a clean image with three objects, the first row is the Rada *et al.* results, and the second row is our proposed model results with $dt = 0.001$. First column: Image with markers points and the initial zero level set contours. The second, third, fourth, and fifth columns are the local, global, segmented features and local+global comparison respectively.

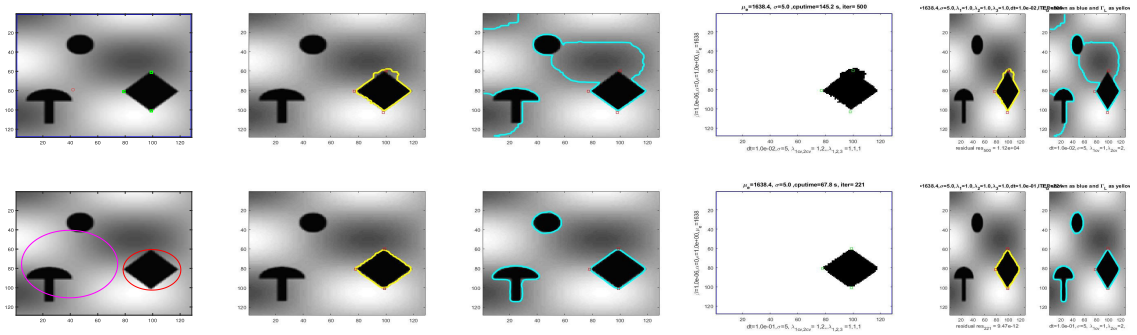

FIGURE 4. The first row is the Rada *et al.* results and the second row is our proposed model results with $dt = 0.01$. First column: Image with markers points and the initial zero level set contours. The second, third, fourth, and fifth columns are the local, global, segmented features and local+global comparison of the proposed model with Rada *et al.* respectively.

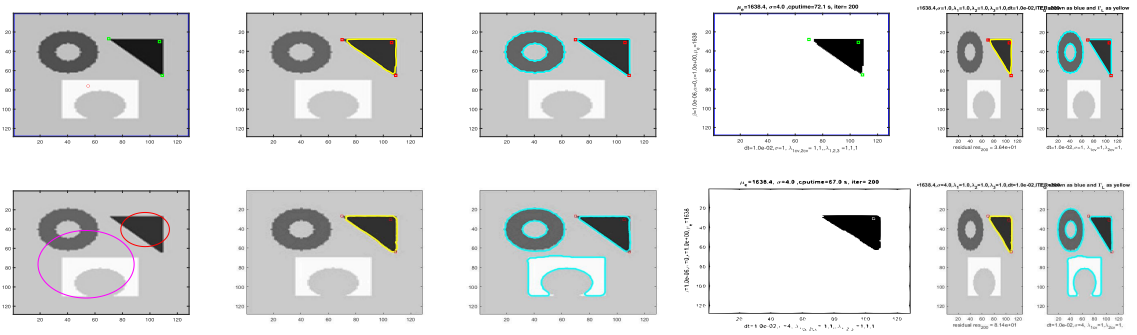

FIGURE 5. The first row is the Rada *et al.* results and the second row is our proposed model results with $dt = 0.001$. First column: Image with markers points and the initial zero level set contours. The second, third, fourth, and fifth columns are the local, global, segmented features and local+global comparison of the proposed model with Rada *et al.* respectively.

The choices of parameters and the initialization of the initial level are the same as for [31] and [19]. Further, we divide this section as follows:

A. TEST SET-1: ROBUSTNESS OF THE PROPOSED MODEL

Test Set-1 consists of experimental results on different images of our proposed model. In Figure 1, the first-row containing images with many features, that is the tomographic image taken from Furat *et al.* [37] and the medical image. The second row is their successful local segmentation results and the third row is their segmented features. On these images, we test the proposed model where one object is to be selected. These show better selective segmentation results. Similarly, Figure 2 demonstrates the performance of the proposed method for Image with a noise (salt and pepper noise) density of 0.02. For example: (a-c) Noisy images with initial contour, (d-f) successful local segmentation results and (g-i) segmented features with $dt = 0.2$.

B. TEST SET-2: LOCAL AND GLOBAL COMPARISON WITH RADA et al.

In Test Set-2, we compare our model locally and globally with Rada *et al.* [31] for 10 different images. Figure 3 is the comparison for a simple clean image, Figs. 4, 7 are

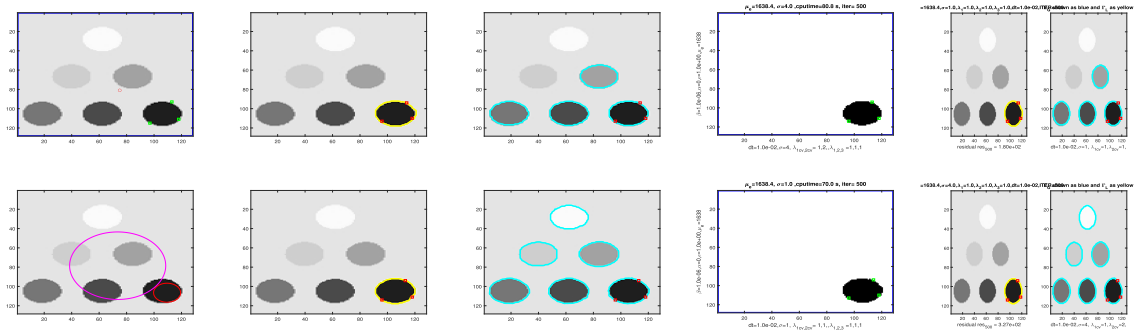

FIGURE 6. The first row is the Rada *et al.* results and the second row is our proposed model results with $dt = 0.01$. First column: Image with markers points and the initial zero level set contours. The second, third, fourth, and fifth columns are the local, global, segmented features and local+global comparison of the proposed model with Rada *et al.* respectively.

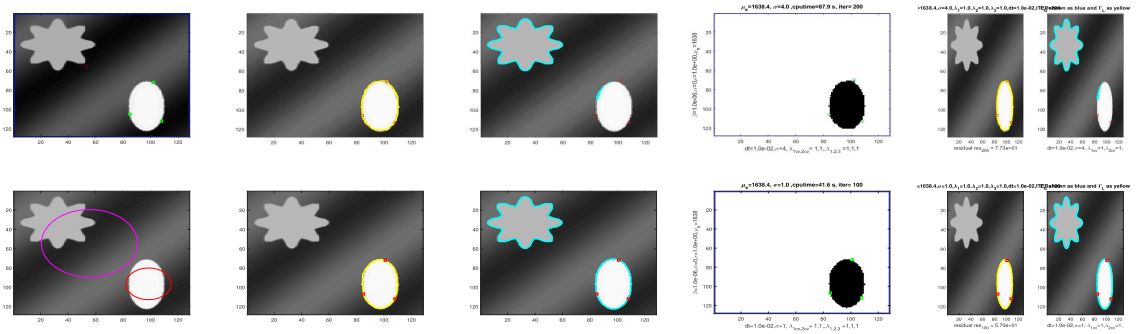

FIGURE 7. The first row is the Rada *et al.* results and the second row is our proposed model results with $dt = 0.01$. First column: Image (background intensity is in-homogeneous) with markers points and the initial zero level set contours. The second, third, fourth, and fifth columns are the local, global, segmented features and local+global comparison of the proposed model with Rada *et al.* respectively.

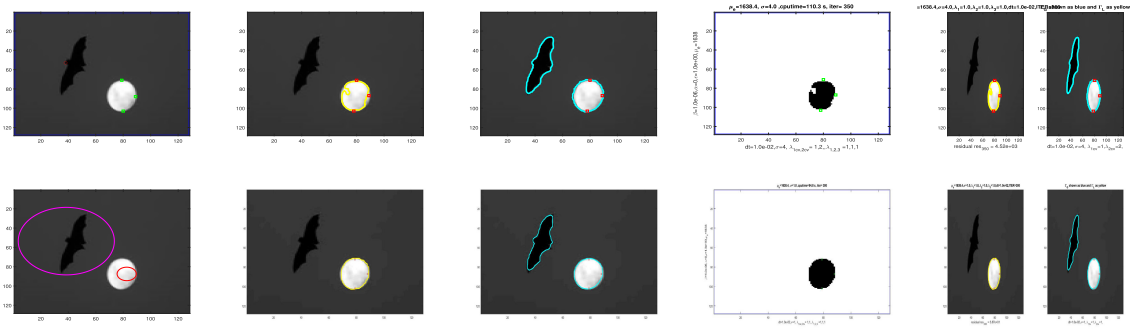

FIGURE 8. The first row is the Rada *et al.* results and the second row is our proposed model results with $dt = 0.01$. First column: Image with markers points and the initial zero level set contours. The second, third, fourth, and fifth columns are the local, global, segmented features and local+global comparison of the proposed model with Rada *et al.* respectively.

for images with background intensities are in-homogeneous, Figs. 5, 6, 8 are for images having objects with different intensities, Figs. 9, 10 and 11 are for medical images having the intensity difference is small between the object and its neighbor and Figure 12 for a noisy image. Better performance can be seen in all these test as compare to Rada *et al.* [31]. Table 1, which is CPU time and iterations comparisons of the proposed model and Rada *et al.* [31] shows that the proposed model is more efficient than the other.

C. TEST SET-3: SELECTIVE COMPARISON WITH MABOOD et al. AND LIU et al.

For the same images as in Test Set-2 and different cases with respect to intensity in-homogeneity Figure 13, are the comparison of our proposed model with the existing models Liu *et al.* [33] and Mabood *et al.* [32]. Better performance can be seen of our proposed model, while Liu *et al.* is not working for these images, and the Mabood *et al.* results are not good.

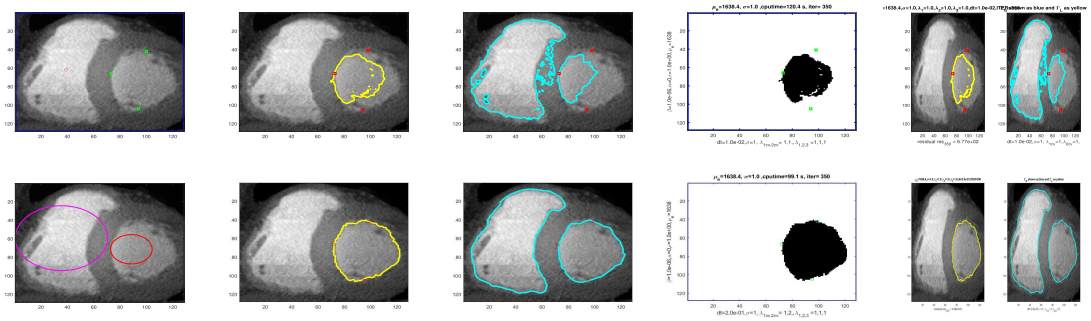

FIGURE 9. The first row is the Rada *et al.* results and the second row is our proposed model results with $dt = 0.02$. First column: Medical image (foreground intensity is in-homogeneous) with markers points and the initial zero levels set contours. The second, third, fourth, and fifth columns are the local, global, segmented features and local+global comparison of the proposed model with Rada *et al.* respectively.

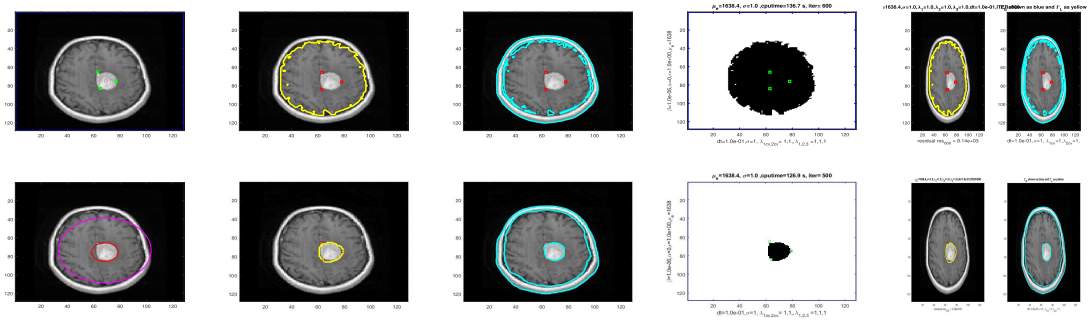

FIGURE 10. The first row is the Rada *et al.* results and the second row is our proposed model results with $dt = 0.01$. First column: Medical image (the foreground intensity is in-homogeneous) with markers points and the initial zero level set contours. The second, third, fourth, and fifth columns are the local, global, segmented features and local+global comparison of the proposed model with Rada *et al.*, respectively.

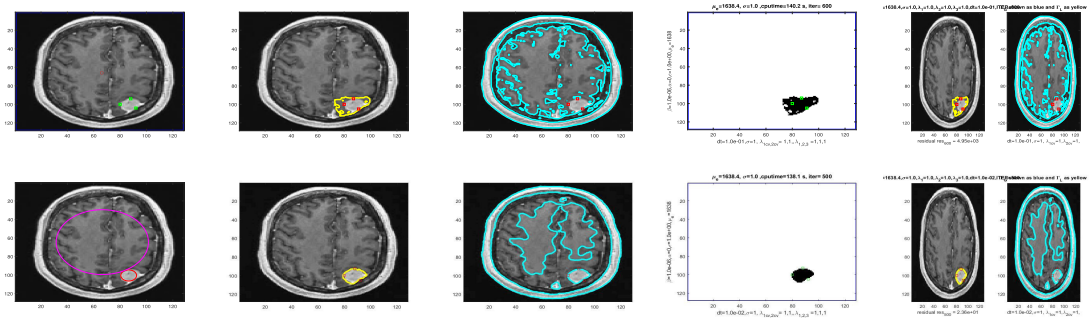

FIGURE 11. The first row is the Rada *et al.* results and the second row is our proposed model results with $dt = 0.01$. First column: Medical image (the foreground intensity is in-homogeneous) with markers points and the initial zero level set contours. The second, third, fourth, and fifth columns are the local, global, segmented features and local+global comparison of the proposed model with Rada *et al.*, respectively.

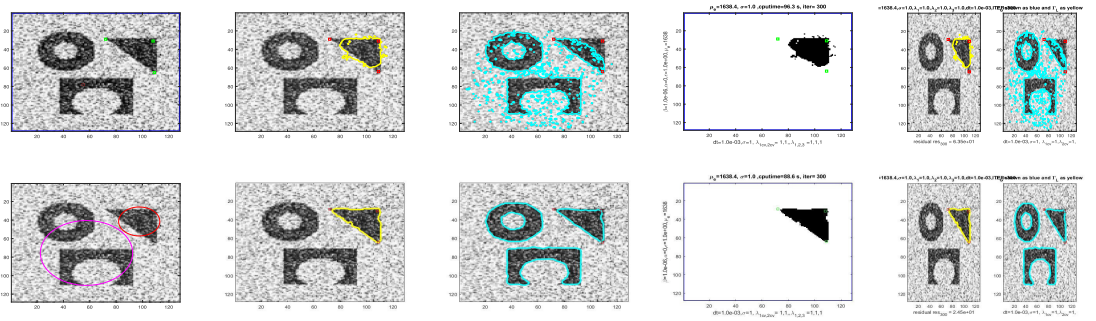

FIGURE 12. The first row is the Rada *et al.* results and the second row is our proposed model results with $dt = 0.001$. First column: Noisy image (with 20 percent Gaussian noise) with markers points and the initial zero level set contours. The second, third, fourth, and fifth columns are the local, global, segmented features and local+global comparison of the proposed model with Rada *et al.*, respectively.

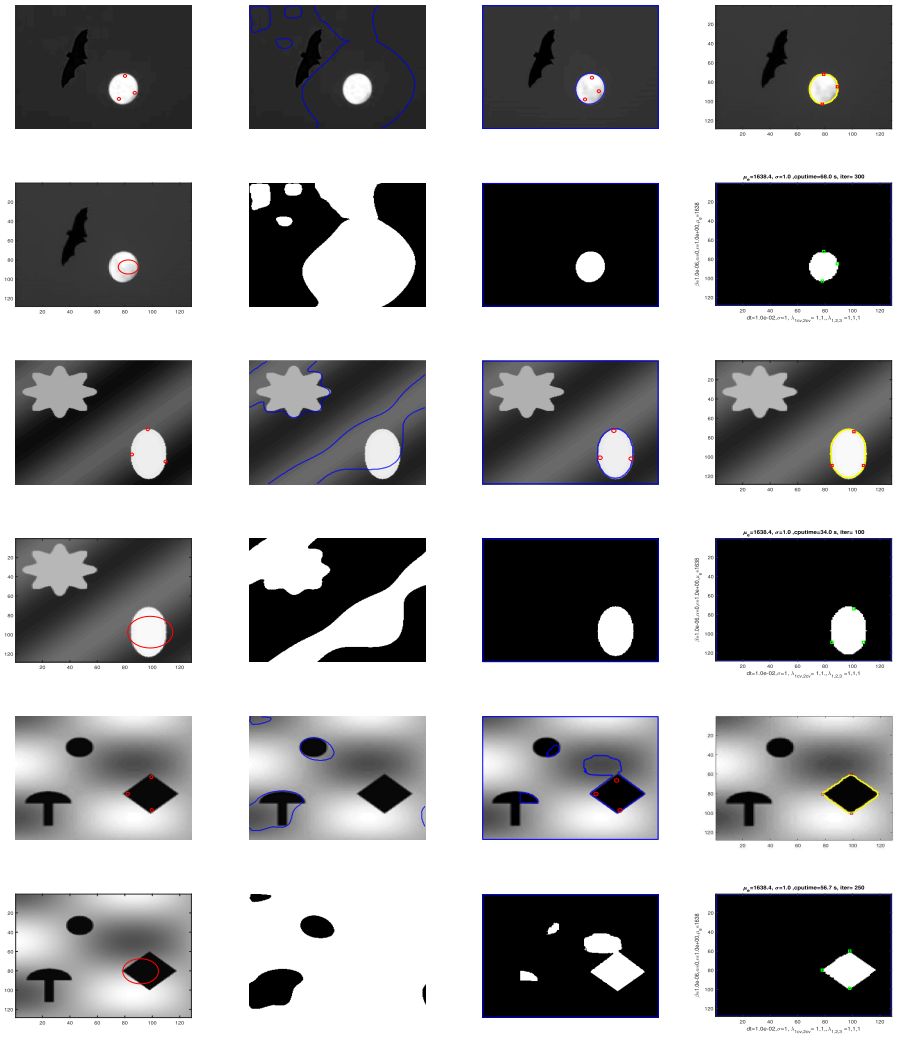

FIGURE 13. First column: Image with markers points and the initial zero level set contour. The second, third, and fourth columns are the segmentation results of Liu *et al.*, Mabood *et al.* and our model, respectively, with $dt = 0.01$.

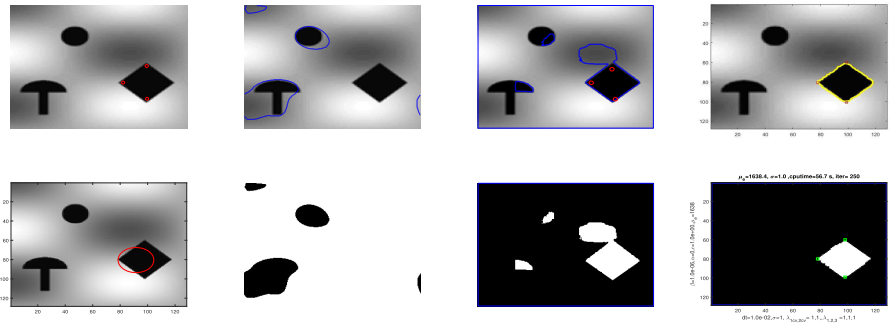

FIGURE 14. First coloumn: Image with markers points and the initial zero level set contour. The second, third, and forth columns are the segmentation results of Liu *et al.*, Mabood *et al.* and our model, respectively, with $dt = 0.01$.

D. QUANTITATIVE ANALYSIS

To ensure the transparency of the experimental analysis we use the Jaccard ans Sϕrensen-Dice similarity similarities indices. Let I_S is the segmented result found by the model algorithm and I_G is the ground truth of the same image.

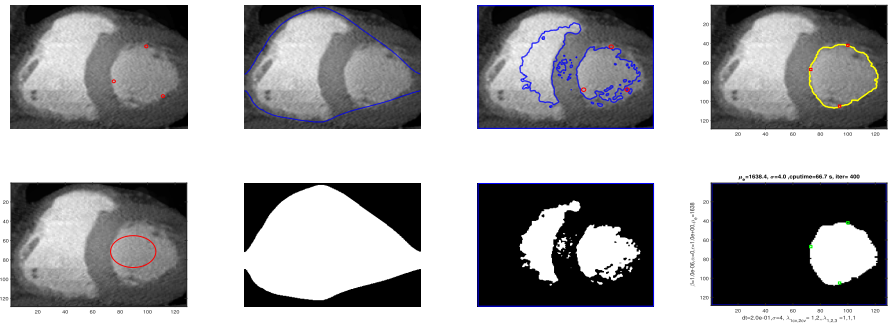

FIGURE 15. First column: Medical image with markers points and the initial zero level set contour. The second, third, and fourth columns are the segmentation results of Liu *et al.*, Mabood *et al.* and our model, respectively, with $dt = 0.2$.

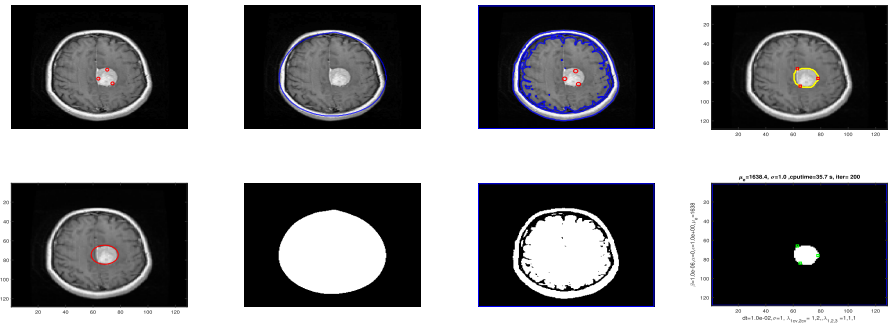

FIGURE 16. First column: Medical image with markers points and the initial zero level set contour. The second, third, and fourth columns are the segmentation results of Liu *et al.*, Mabood *et al.* and our model, respectively, with $dt = 0.1$.

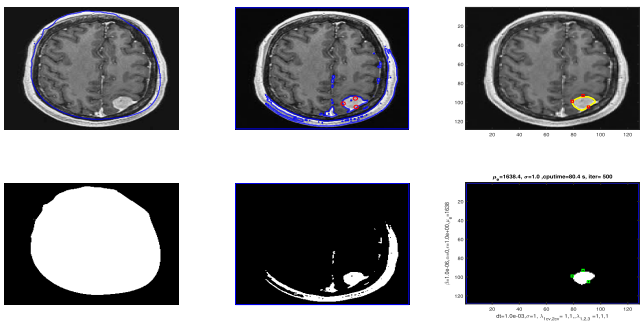

FIGURE 17. First, second, and third columns are the segmentation results of Liu *et al.*, Mabood *et al.* and our model, respectively, with $dt = 0.01$.

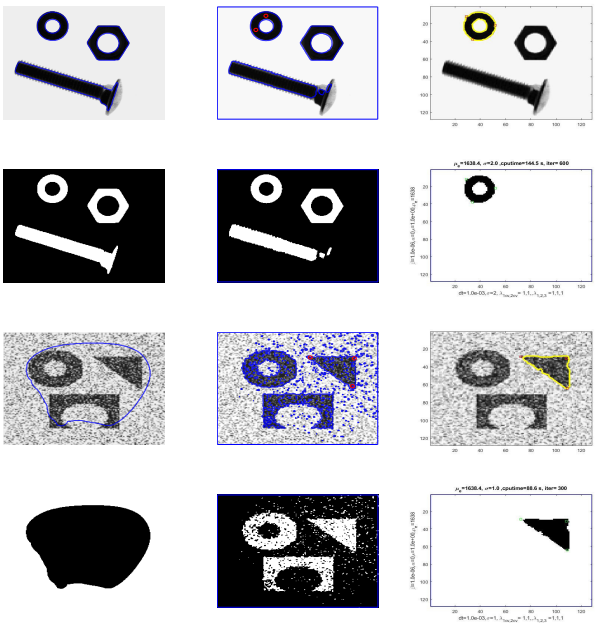

FIGURE 18. First,second, and third columns are the segmentation results of Liu *et al.*, Mabood *et al.* and our model, respectively, with $dt = 0.001$ for the first and $dt = 0.2$ for the second image.

1) JACCARD SIMILARITY

The Jaccard similarity coefficient computed as:

$$JS(I_S, I_G) = \frac{|I_S \cap I_G|}{|I_S \cup I_G|},$$

where $|\ .\ |$ denotes the cardinality. The range of the Jaccard value is in $[0, 1]$. The higher Jaccard value shows better segmentation result.

2) SϕRENSEN-DICE SIMILARITY

The Sϕrensen-Dice similarity is computed as

$$D(I_S, I_G) = \frac{2|I_S \cap I_G|}{|I_S| + |I_G|}.$$

The Sϕrensen-Dice similarity value is also in $[0, 1]$. The higher Dice value shows better segmentation result.

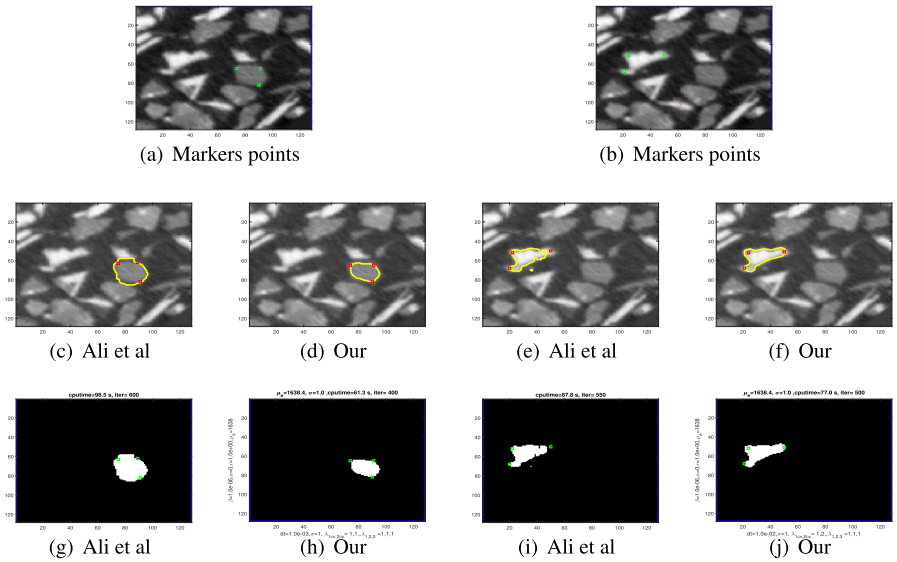

(a) Markers points (b) Markers points

(c) Ali et al (d) Our (e) Ali et al (f) Our

(g) Ali et al (h) Our (i) Ali et al (j) Our

FIGURE 19. Comparison of our proposed model with Ali *et al.* [38] on Tomographic image. (a), (b) are the markers points, (c), (e), (g) and (i) are the results of Ali *et al.*, while (d), (f), (h) and (j) are the results of our proposed model. It is clear that our model is robust and more efficient as compared to Ali *et al.*

TABLE 2. Jaccard similarity coefficients for Liu *et al.* [33], Mabood *et al.* [32], Rada *et al.* [31], Ali *et al.* [38] and the proposed model on 10 different images.

Liu et al.	Mabood et al.	Rada et al.	Ali et al.	proposed model
0.71 ± 0.75	0.88 ± 0.047	0.94 ± 0.073	0.91 ± 0.083	0.98 ± 0.083

TABLE 3. Sϕrensen-Dice similarity for Liu *et al.* [33], Mabood *et al.* [32], Rada *et al.* [31], Ali *et al.* [38] and the proposed model on 10 different images.

Liu et al.	Mabood et al.	Rada et al.	Ali et al.	proposed model
0.71 ± 0.78	0.90 ± 0.056	0.80 ± 0.069	0.93 ± 0.081	0.97 ± 0.081

Table 2 shows the JS coefficients comparison and Table 3 shows Sϕrensen-Dice coefficients comparison of our proposed model with other competing models Liu *et al.* [33], Mabood *et al.* [32] and Rada *et al.* [31]. The results are obtained from experiments on 10 different images suitable for interactive segmentation with a pre-labeled ground truth consisting of the mean of the labeled ground truth. It can be observed that Rada *et al.* produced relatively better results compared to Liu *et al.* and Mabood *et al.*, but for a high noisy or low intensity image it loses the details. From the results it is clear that our model perform better than the other competing models.

VI. CONCLUSION AND FUTURE WORK

This article mainly focuses on designing a new variational model with dual-level set functions for local and global segmentation which performs better segmentation for images having multi-region, multi-object, noisy, and intensity in-homogeneity. Moreover, the new model is efficient in medical and synthetic images having objects with non-uniform features. Experimental results show that the new model is faster, efficient and reliable than the models Rada *et al.* [31] (global and selective segmentation), Mabood *et al.* [32], Liu *et al.* [33] (selective segmentation). To achieve proper picture segmentation in the presence of noise and outliers, outliers must be identified and isolated during the denoising pre-processing or appropriate limitations must be imposed on the segmentation framework. For accurate picture segmentation in the future, we will apply appropriate eliminating outliers requirements backed by a well-designed theory in a variational framework.

ACKNOWLEDGMENT

The code of the proposed method will be provided for research purposes if requested via email.

REFERENCES

[1] G. Aubert and P. Kornprobst, *Mathematical Problems in Image Processing*. New York, NY, USA: Springer, 2002.
[2] T. F. Chan and L. A. Vese, "Active contours without edges," *IEEE Trans. Image Process.*, vol. 10, no. 2, pp. 266–277, Feb. 2001.
[3] M. Kass, A. Witkin, and D. Terzopoulos, "Snakes: Active contour models," *Int. J. Comput. Vis.*, vol. 1, no. 1, pp. 321–331, Jan. 1988.
[4] R. Adams and L. Bischof, "Seeded region growing," *IEEE Trans. Pattern Anal. Mach. Intell.*, vol. 16, no. 6, pp. 641–647, Jun. 1994.
[5] S. W. Zucker, "Region growing: Childhood and adolescence," *Comput. Graph. Image Process.*, vol. 5, no. 3, pp. 382–399, Sep. 1976.
[6] J. Malik, S. Belongie, T. Leung, and J. Shi, "Contour and texture analysis for image segmentation," *Int. J. Comput. Vis.*, vol. 43, no. 1, pp. 7–27, Jun. 2001.

[7] D. Sen and S. K. Pal, "Histogram thresholding using fuzzy and rough measures of association error," *IEEE Trans. Image Process.*, vol. 18, no. 4, pp. 879–888, Apr. 2009.

[8] L. Vincent and P. Soille, "Watersheds in digital spaces: An efficient algorithm based on immersion simulations," *IEEE Trans. Pattern Anal. Mach. Intell.*, vol. 13, no. 6, pp. 583–598, Jun. 1991.

[9] D. Mumford and J. Shah, "Optimal approximations by piecewise smooth functions and associated variational problems," *Commun. Pure Appl. Math.*, vol. 42, no. 5, pp. 577–685, Jul. 1989.

[10] R. Ronfard, "Region-based strategies for active contour models," *Int. J. Comput. Vis.*, vol. 13, no. 2, pp. 229–251, 1994.

[11] L. A. Vese and T. F. Chan, "A multiphase level set framework for image segmentation using the Mumford and Shah model," *Int. J. Comput. Vis.*, vol. 50, no. 3, pp. 271–293, Dec. 2002.

[12] V. Caselles, R. Kimmel, and G. Sapiro, "Geodesic active contours," *Int. J. Comput. Vis.*, vol. 22, no. 1, pp. 61–79, 1997.

[13] S. Kichenassamy, A. Kumar, P. Olver, and A. Yezzi, "Snake: Conformal curvature flows: From phase transitions to active vision," *Arch. Rational Mech. Anal.*, vol. 134, no. 3, pp. 275–301, 1996.

[14] C. Li, C. Xu, C. Gui, and M. D. Fox, "Level set evolution without re-initialization: A new variational formulation," in *Proc. IEEE Comput. Soc. Conf. Comput. Vis. Pattern Recognit. (CVPR)*, vol. 1, Jun. 2005, pp. 430–436.

[15] C. Rother, V. Kolmogorov, and A. Blake, "'GrabCut' interactive foreground extraction using iterated graph cuts," *ACM Trans. Graph.*, vol. 23, no. 3, pp. 309–314, 2004.

[16] X. Bai and G. Sapiro, "A geodesic framework for fast interactive image and video segmentation and matting," in *Proc. IEEE 11th Int. Conf. Comput. Vis.*, Oct. 2007, pp. 1–8.

[17] L. Grady, "Random walks for image segmentation," *IEEE Trans. Pattern Anal. Mach. Intell.*, vol. 28, no. 11, pp. 1768–1783, Nov. 2006.

[18] C. Le Guyader and C. Gout, "Geodesic active contour under geometrical conditions: Theory and 3D applications," *Numer. Algorithms*, vol. 48, nos. 1–3, pp. 105–133, Jul. 2008.

[19] N. B. A. K. Chen, "Image selective segmentation under geometrical constraints using an active contour approach," *Commun. Comput. Phys.*, vol. 7, no. 4, pp. 759–778, Jun. 2010.

[20] T. N. A. Nguyen, J. Cai, J. Zhang, and J. Zheng, "Robust interactive image segmentation using convex active contours," *IEEE Trans. Imag. Process.*, vol. 21, no. 8, pp. 3734–3743, Aug. 2012.

[21] T. Goldstein, X. Bresson, and S. Osher, "Geometric applications of the split Bregman method: Segmentation and surface reconstruction," *J. Sci. Comput.*, vol. 45, no. 1, pp. 272–293, Oct. 2010.

[22] D. Adalsteinsson and J. A. Sethian, "A fast level set method for propagating interfaces," *J. Comput. Phys.*, vol. 118, no. 2, pp. 269–277, 1995.

[23] T. F. Chan, B. Y. Sandberg, and L. A. Vese, "Active contours without edges for vector-valued images," *J. Vis. Commun. Image Represent.*, vol. 11, no. 2, pp. 130–141, 2000.

[24] T. F. Chan and L. A. Vese, "An efficient variational multiphase motion for the Mumford–Shah segmentation model," in *Proc. 34th Asilomar Conf. Signals, Syst. Comput.*, vol. 1, 2000, pp. 490–494.

[25] S. Osher and R. Fedkiw, *Level Set Methods and Dynamic Implicit Surfaces*, vol. 153. New York, NY, USA: Springer, 2006, doi: 10.1007/b98879.

[26] J. A. Sethian, *Level Set Methods and Fast Marching Methods: Evolving Interfaces in Computational Geometry, Fluid Mechanics, Computer Vision and Material Science*, vol. 3. Cambridge, U.K.: Cambridge Univ. Press, 1999.

[27] H. Ali, N. Badshah, K. Chen, G. A. Khan, and N. Zikria, "Multiphase segmentation based on new signed pressure force functions and one level set function," *TURKISH J. Electr. Eng. Comput. Sci.*, vol. 25, no. 4, pp. 2943–2955, Jul. 2017.

[28] T. F. Chan and J. Shen, *Image Processing and Analysis: Variational, PDE, Wavelet, and Stochastic Methods*. Philadelphia, PA, USA: SIAM Publications, Jan. 2005.

[29] F. Li, M. K. Ng, T. Y. Zeng, and C. Shen, "A multiphase image segmentation method based on fuzzy region competition," *SIAM J. Imag. Sci.*, vol. 3, no. 3, pp. 277–299, 2010.

[30] A. Mitiche and I. Ben-Ayed, *Variational and Level Set Methods in Image Segmentation*. Berlin, Germany: Springer, 2010, doi: 10.1007/978-3-642-15352-5.

[31] L. Rada and K. Chen, "A new variational model with dual level set functions for selective segmentation," *Commun. Comput. Phys.*, vol. 12, no. 1, pp. 261–283, Jul. 2012.

[32] L. Mabood, H. Ali, N. Badshah, K. Chen, and G. A. Khan, "Active contours textural and inhomogeneous object extraction," *Pattern Recognit.*, vol. 55, pp. 87–99, Jul. 2016.

[33] C. Liu, M. K.-P. Ng, and T. Zeng, "Weighted variational model for selective image segmentation with application to medical images," *Pattern Recognit.*, vol. 76, pp. 367–379, Apr. 2018.

[34] S. Niu, Q. Chen, L. de Sisternes, Z. Ji, Z. Zhou, and D. L. Rubin, "Robust noise region-based active contour model via local similarity factor for image segmentation," *Pattern Recognit.*, vol. 61, pp. 104–119, Jan. 2017.

[35] T. Lu, P. Neittaanmäki, and X.-C. Tai, "A parallel splitting up method and its application to Navier–Stokes equations," *Appl. Math. Lett.*, vol. 4, no. 2, pp. 25–29, 1991.

[36] J. Weickert, B. M. T. H. Romeny, and M. A. Viergever, "Efficient and reliable schemes for nonlinear diffusion filtering," *IEEE Trans. Image Process.*, vol. 7, no. 3, pp. 398–410, Mar. 1998.

[37] O. Furat, M. Wang, M. Neumann, L. Petrich, M. Weber, C. E. Krill, and V. Schmidt, "Machine learning techniques for the segmentation of tomographic image data of functional materials," *Frontiers Mater.*, vol. 6, p. 145, Jun. 2019.

[38] H. Ali, S. Faisal, K. Chen, and L. Rada, "Image-selective segmentation model for multi-regions within the object of interest with application to medical disease," *Vis. Comput.*, vol. 37, no. 5, pp. 939–955, May 2021.

[39] A. Mondal, S. Ghosh, and A. Ghosh, "Robust global and local fuzzy energy based active contour for image segmentation," *Appl. Soft Comput.*, vol. 47, pp. 191–215, Oct. 2016.

[40] K. S. Chuang, H. L. Tzeng, S. Chen, J. Wu, and T. J. Chen, "Fuzzy c-means clustering with spatial information for image segmentation," *Comput. Med. Imag. Graph.*, vol. 30, no. 1, pp. 9–15, Jan. 2006.

[41] B. K. Tripathy, A. Basu, and S. Govel, "Image segmentation using spatial intuitionistic fuzzy c means clustering," in *Proc. IEEE Int. Conf. Comput. Intell. Comput. Res.*, Dec. 2014, pp. 1–5.

[42] Y. Wu and C. He, "A convex variational level set model for image segmentation," *Signal Process.*, vol. 106, pp. 123–133, Jan. 2015.

AFZAL RAHMAN received the M.Sc. degree from the Department of Mathematics, University of Peshawar, Pakistan, in 2010, and the M.S. degree in applied mathematics from Trento University, in 2015. He is currently pursuing the Ph.D. degree with the University of Peshawar. His research interests include variational models and computational algorithms, image processing, machine learning, image segmentation, image inpainting, and medical image analysis.

HAIDER ALI received the M.Sc. degree in mathematics from the University of Peshawar, Pakistan, in 2007, the M.S. degree in applied mathematics (variational models in image processing) from the University of Engineering and Technology Peshawar, in 2012, and the Ph.D. degree in applied mathematics (variational models in image processing) from the University of Peshawar, in 2016. Since 2010, he has been a Lecturer and a Researcher at the University of Peshawar. His research interests include image processing, medical image analysis, robotics, machine learning, segmentation, and registration using PDEs and variational methods.

NOOR BADSHAH received the B.Sc. and M.Sc. degrees in mathematics from the University of Peshawar and the Ph.D. degree in applied mathematics (fast algorithms for image segmentation and variational models) from the Department of Mathematical Sciences, University of Liverpool, Liverpool, U.K. His research interests include fast algorithms for variational image processing models and medical image analysis.

LAVDIE RADA received the B.Sc. degree in mathematics from the Natural Sciences Faculty in Tirana, Albania, the M.Sc. degree in applied mathematics from the Polytechnic University of Tirana, Albania, and the Ph.D. degree in fast iterative methods for variational models of image segmentation from the Department of Mathematical Sciences, University of Liverpool, Liverpool, U.K. She has been a Lecturer with the Engineering and Natural Sciences Faculty, Bahcesehir University, Istanbul, since 2014. Her research interests include developing elective solvers for variational image processing models continued in a Postdoctoral Fellowship at the Faculty of Engineering and Natural Sciences, Sabanci University, Istanbul, Turkey.

AYAZ ALI KHAN received the Ph.D. degree in computer science from Abdul Wali Khan University Mardan, Pakistan. He is currently an Assistant Professor with the Department of Computer Science, University of Lakki Marwat, Pakistan. He has deep understanding of the theoretical computer science and data analysis. Furthermore, he also owns deep understanding of various statistical techniques which are, largely, used in applied research. His research has appeared in several international conferences, journals, and transactions of repute. His research interests include cloud computing, mobile edge clouds, the Internet of Things (IoT), performance, energy efficiency, algorithms, and resource management.

HAMEED HUSSAIN received the bachelor's degree in information technology from Gomal University Dera Ismail Khan, Pakistan, in 2007, and the M.S. and Ph.D. degrees in computer science from the COMSATS Institute of Information Technology (CIIT), Pakistan, in 2009 and 2017, respectively. He is an Active Researcher. He is the author of several international publications. His research interests include optimization, machine learning, fog and edge computing, real-time systems, resource allocation, and load balancing in high-performance computing.

MUHAMMAD ZAKARYA (Senior Member, IEEE) received the Ph.D. degree in computer science from the University of Surrey, Guildford, U.K. He is currently a Lecturer with the Department of Computer Science, Abdul Wali Khan University Mardan (AWKUM), Pakistan. He is the Program Director of the iFuture: a leading research group at AWKUM which has research collaboration with the CLOUDS Laboratory, The University of Melbourne, Australia, and the IoT Laboratory, Cardiff University, U.K. He has deep understanding of the theoretical computer science and data analysis. Furthermore, he also owns deep understanding of various statistical techniques which are, largely, used in applied research. His research has appeared in several international conferences, journals, and transactions of repute. His research interests include cloud computing, mobile edge clouds, the Internet of Things (IoT), performance, energy efficiency, algorithms, and resource management. He is a TPC member of few prestigious international conferences, including CCGrid, GECON, and UCC. He is also an Associate Editor of IEEE Access journal and *Journal of Cloud Computing* (Springer). He is also a Guest Editor of *Cluster Computing* journal (Springer). He has been listed in the world's top 2% scientists list for 2020.

AFTAB AHMED received the Ph.D. degree in electronic engineering from the University of York, U.K., in 2019. He is currently a Lecturer with the Computer Science Department, Abdul Wali Khan University Mardan, Pakistan. His research work is related to improvement in performance in ultra-dense high-capacity networks. His other research interests include radio resource management, topology management to improve system performance and overall energy efficiency in ultra-dense high-capacity wireless networks, and machine learning.

IZAZ UR RAHMAN received the Ph.D. degree in computer science from the Department of Electronic and Computer Engineering, Brunel University, U.K. He is currently an Assistant Professor with the Department of Computer Science, Abdul Wali Khan University Mardan, Pakistan. His research interests include power systems, optimization algorithms, the Internet of Things, and artificial intelligence.

MUSHTAQ RAZA received the Ph.D. degree in computer science from the Faculty of Sciences, University of Porto, Portugal, with a focus on software engineering. He is currently an Assistant Professor of computer science with Abdul Wali Khan University Mardan (AWKUM) and a Research Collaborator with the Institute for Systems and Computer Engineering, Technology and Science (INESC TEC), Porto. Previously, he was a Researcher with INESC TEC and has published more than 20 papers in renowned journals and conferences in software engineering. His research interests include software process improvement, machine learning, big data analysis, software engineering, and the Internet of Things (IoT). He is also a Program Committee Member of ICSSP, top conference in software engineering, and a Focal Person of the National Technology Fund with AWKUM.

MUHAMMAD HALEEM is currently an Assistant Professor with the Department of Computer Science, Faculty of Engineering, Kardan University, Kabul, Afghanistan. His research interests include the Internet of Things, machine learning, and data analytics.